J|A|C|S
ARTICLES
Published on Web 04/18/2006

Clay−Fulleropyrrolidine Nanocomposites

Dimitrios Gournis,*[,†,‡] Luboš Jankovič,[†] Enrico Maccallini,[‡] Darja Benne,[‡] Petra Rudolf,*[,‡] Jean-François Colomer,[§] Chloé Sooambar,[||] Vasilios Georgakilas,[#] Maurizio Prato,*[,||] Marianna Fanti,[£] Francesco Zerbetto,*[,£] Ginka H. Sarova,[+] and Dirk M. Guldi*[,+]

Contribution from the Department of Materials Science and Engineering, University of Ioannina, GR-45110 Ioannina, Greece, Materials Science Centre, University of Groningen, Nijenborgh 4, NL-9747 AG Groningen, The Netherlands, Laboratoire de Résonance Magnétique Nucléaire, Facultés Universitaires Notre-Dame de la Paix, 61 rue de Bruxelles, B-5000 Namur, Belgium, Dipartimento di Scienze Farmaceutiche, Università di Trieste, Piazzale Europa 1, I-34127 Trieste, Italy, Institute of Materials Science, NCSR "DEMOKRITOS", Ag. Paraskevi-Attikis, GR-15310 Athens, Greece, Dipartimento di Chimica "G. Ciamician", Università di Bologna, V. F. Selmi 2, I-40126 Bologna, Italy, and Institute for Physical Chemistry, Friedrich-Alexander-Universität Erlangen-Nürnberg, Egerlandstr. 3, D-91058 Erlangen, Germany

Received November 23, 2005; E-mail: dgourni@cc.uoi.gr; p.rudolf@rug.nl; prato@units.it; francesco.zerbetto@unibo.it; guldi@chemie.uni-erlangen.de

Abstract: In this work, we describe the insertion of a water-soluble bisadduct fulleropyrrolidine derivative into the interlayer space of three layered smectite clays. The composites were characterized by a combination of powder X-ray diffraction, transmission electron microscopy, X-ray photoemission and FTIR spectroscopies, and laser flash photolysis measurements. The experiments, complemented by computer simulations, give insight into the formation process, structural details, and properties of the fullerene/clay nanocomposites. The reported composite materials constitute a new hybrid system, where C_{60} differs from its crystals or its solutions, and open new perspectives for the design and construction of novel C_{60}-based organic/clay hybrid materials.

Introduction

Smectite clays are a class of layered aluminosilicate minerals with a unique combination of swelling, intercalation, and ion exchange properties that make them valuable nanostructures in diverse fields.[1,2] Their structure consists of an octahedral alumina layer fused between two tetrahedral silica layers. Smectite clays have a cation exchange capacity, which depends on the substitution of low-valent atoms, such as Mg^{2+} for Al^{3+} in the octahedral sheet, and Al^{3+} for Si^{4+} in the tetrahedral sites. As a consequence, the layers are negatively charged and neutrality is obtained, for example, by hydrated cations present in the galleries. The intercalation process in these systems is equivalent to ion exchange and, unlike for intercalation compounds of graphite, it does not involve necessarily charge transfer between the guest and host species. These materials have the natural ability to adsorb organic or inorganic guest cationic species (and even neutral molecules) from solutions, and it is this cation "storage" that gives unique properties to clay minerals, which can be used as catalysts,[3] templates[4] in organic synthesis, or as building stones for composite materials.[5−7] The nature of the microenvironment between the aluminosilicate sheets regulates the topology of the intercalated molecules and affects possible supramolecular rearrangements or reactions, such as self-assembling processes that are usually not easily controlled in the solution phase.[5−7]

Fullerenes have been extensively studied during the past decade.[8] Their physical and chemical properties have been scrutinized, and a high number of organic derivatives and composites have been prepared and characterized. Drawbacks

[†] University of Ioannina.
[‡] University of Groningen.
[§] Facultés Universitaires Notre-Dame de la Paix.
[||] Università di Trieste.
[#] NCSR "DEMOKRITOS".
[£] Università di Bologna.
[+] Friedrich-Alexander-Universität Erlangen-Nürnberg.

(1) (a) Pinnavaia, T. J. *Science* **1983**, *220*, 365. (b) Konta, J. *Appl. Clay Sci.* **1995**, *10*, 275. (c) Lagaly, G. *Solid State Ionics* **1986**, *22*, 43.
(2) Newman, A. C. D. *Chemistry of Clays and Clay Minerals*; Mineralogical Society Monograph, No. 6; Longman: London, 1987.
(3) (a) Ballantine, J. A. *NATO-ASI Ser. C* **1986**, *165*, 197. (b) Cornelis, A.; Laszlo, P. *NATO-ASI Ser. C* **1986**, *165*, 213.
(4) (a) Georgakilas, V.; Gournis, D.; Petridis, D. *Angew. Chem., Int. Ed.* **2001**, *40*, 4286. (b) Georgakilas, V.; Gournis, D.; Bourlinos, A. B.; Karakassides, M. A.; Petridis, D. *Chem.−Eur. J.* **2003**, *9*, 3904.
(5) Theng, B. K. G. *The Chemistry of Clay Organic Reactions*; Adam Hilger: London, 1974.
(6) (a) Kloprogge, J. T. *J. Porous Mater.* **1998**, *5*, 5. (b) Gil, A.; Gandia, L. M.; Vicente, M. A. *Catal. Rev. Sci. Eng.* **2000**, *42*, 145. (c) Ma, Y.; Tong, W.; Zhou, H.; Suib, S. L. *Microporous Mesoporous Mater.* **2000**, *37*, 243. (d) Ohtsuka, K. *Chem. Mater.* **1997**, *9*, 2039.
(7) Shichi, T.; Takagi, K. *J. Photochem. Photobiol. C* **2000**, *1*, 113.
(8) (a) Prato, M.; Martin, N. *J. Mater. Chem.* **2002**, *12*, 1931. (b) Prassides, K. *Physics and Chemistry of the Fullerenes*; Kluwer Academic: Dordrecht, The Netherlands, 1994. (c) Kroto, H. W. *The Fullerenes: New Horizons for the Chemistry, Physics and Astrophysics of Carbon*; Cambridge University Press: Cambridge, 1997. (d) Hirsch, A. *Fullerenes and Related Structures*; Springer: Berlin, 1999. (e) Kadish, K. M.; Ruoff, R. S. *Fullerenes: Chemistry, Physics and Technology*; Wiley-Interscience: New York, 2000. (f) Diederich, F.; Thilgen, C. *Science* **1996**, *271*, 317.

 10.1021/ja0579661 CCC: $33.50

for their use in several applications, especially in those based on optical and electronic properties, arise from difficulties in processibility and incorporation into various solid matrices, such as polymers, glasses, metals, and other materials, since the low solubility of fullerenes in different solvents is a serious obstacle. Organic derivatization of fullerenes can help solubilization both in organic solvents and in water and also influence their properties.[9] The chemical functionalization of the fullerene sphere produces a large number of different derivatives that combine the desirable properties of C_{60} with the solubilizing power of the side chains. One of the most versatile addition reactions is the [1,3]-dipolar cycloaddition of azomethine ylides, which produces the so-called fulleropyrrolidines, in which the nitrogen and/or carbon atoms in the pyrrolidine ring can be variously functionalized.[10] However, except in few cases,[11] even with very polar functionalizing chains, the water solubility is often very low partly due to aggregation since the spheres tend to stick together in micelle-like aggregates.[12] In principle, one way to avoid aggregation and to increase solubility is to produce polyadducts of C_{60}.[13] In the case of fulleropyrrolidines, bisadduct derivatives of C_{60} with polar fragments, such as oligoethylene glycol chains with positively charged amino groups, showed the highest solubility in aqueous solvents ever reported for fullerene derivatives.[14] The polar chains distribute more or less homogeneously around the spheroid, thus improving the solubility, while the presence of positive charges creates a repulsive effect between the spheres, thus preventing aggregation in aqueous solution.

The incorporation of C_{60} into porous or layered materials is a nontrivial task, and the study of these composites can offer helpful answers concerning the utilization of fullerenes and their derivatives for possible applications. In addition, it can be examined whether fullerene derivatives can form novel structures where the molecules are ordered in one or two dimensions, and how the presence of a molecule changes the basic properties of the bulk material. Moreover, the C_{60}-based organic/clay hybrid materials may possess interesting photophysical characteristics and thus enable the development of photofunctional devices in the form of anisotropic thin films on metallic or glass surfaces.[7] A further challenging goal is the possibility of direct C_{60} functionalization using clays. The 30 double bonds of C_{60} can be easily functionalized in many types of organic reactions. The presence of so many reacting bonds creates numerous isomers and increases the difficulties in the separation and characterization of the products. However, when a fullerene is placed between the clay layers, a part of the cage surface is protected and some double bonds are hidden to any reaction. The interlayer space of clay is therefore expected to induce selective reactivity, while it may also be interesting to study the fullerene reactivity in a microenvironment, such as the interior of the clay. Finally, fullerene derivatives grafted to aluminosilicate layers are attractive for polymer reinforcing applications. One would expect that the combined action of clay and fullerene derivatives in polymer matrices could provide novel functionalities to the resulting composite materials. In particular, the inherent electronic properties of C_{60} as a component of polymer composites could produce materials with enhanced static dissipation, better electromagnetic compatibility, and improved thermal conductivity.

The incorporation of pure C_{60} into porous materials, such as molecular sieves[15,16] and layered double hydroxides (LDH),[17−19] has been extensively studied. Keizer et al.[15] reported the trapping of C_{60} in 13 Å molecular sieves through gas-phase absorption and the occurrence of C_{60}^- radical ions. Hamilton et al.[18] described the incorporation of C_{60} into channel-shape porous sieves VPI-5 from benzene solutions. The composite showed strong white light emission arising from the C_{60} molecules. Finally, Cheng et al.[19] showed that pure C_{60} molecules adsorbed into LDH, with dodecyl sulfate counterions, do not rotate as freely as in the pure solid form. Mehrotra and Giannelis[20] incorporated water-soluble ethylenediamine-functionalized fullerene into mica-type silicate layers through ion exchange.

Recently,[21] we described the insertion and the subsequent behavior of three fulleropyrrolidine monoadduct derivatives, positively charged and slightly soluble in water, into the interlayer space of an aluminosilicate-layered mineral. Organophilic derivatives were intercalated into organically modified clays, while slightly water-soluble fulleropyrrolidines were introduced into the clay galleries through ion exchange. The experiments, complemented by computer simulations, showed that not all the clay−clay platelets are intercalated by the fullerene derivatives (probably due to low solubility of the guest molecules) and that a sizable amount of charge transfer takes place between the host and the guests.

In this work, we report the successful incorporation of a highly water-soluble bisadduct fulleropyrrolidine derivative into three different clays by ion exchange. The clay/fulleropyrrolidine composites were characterized by a combination of powder X-ray diffraction, transmission electron microscopy, X-ray photoemission and FTIR spectroscopies, and laser flash photolysis measurements. The experiments, complemented by computer simulations, give insight into the formation process, structural details, and properties of the fullerene/clay nanocomposites.

Experimental Section

Host Layered Materials. Three different smectites with different particle size and cation exchange capacity were used in this study. The first was a natural Wyoming montmorillonite (SWy-1) obtained from

(9) (a) Prato, M. *J. Mater. Chem.* **1997**, *7*, 1097. (b) Prato, M. *Top. Curr. Chem.* **1999**, *199*, 173. (c) Wudl, F. *J. Mater. Chem.* **2002**, *12*, 1959.
(10) (a) Tagmatarchis, N.; Prato, M. *Synlett* **2003**, 768. (b) Maggini, M.; Scorrano, G.; Prato, M. *J. Am. Chem. Soc.* **1993**, *115*, 9798. (c) Prato, M.; Maggini, M. *Acc. Chem. Res.* **1998**, *31*, 519.
(11) DaRos, T.; Prato, M.; Novello, F.; Maggini, M.; Banfi, E. *J. Org. Chem.* **1996**, *61*, 9070.
(12) Georgakilas, V.; Pellarini, F.; Prato, M.; Guldi, D. M.; Melle-Franco, M.; Zerbetto, F. *Proc. Natl. Acad. Sci. U.S.A.* **2002**, *99*, 5075.
(13) Lamparth, I.; Hirsch, A. *J. Chem. Soc., Chem. Commun.* **1994**, 1727.
(14) Bosi, S.; Feruglio, L.; Milic, D.; Prato, M. *Eur. J. Org. Chem.* **2003**, 4741.
(15) Keizer, P. N.; Morton, J. R.; Preston, K. F.; Sugden, A. K. *J. Phys. Chem.* **1991**, *95*, 7117.
(16) (a) Galletero, M. S.; Garcia, H.; Bourdelande, J. L. *Chem. Phys. Lett.* **2003**, *370*, 829. (b) Lee, C. H.; Lin, T. S.; Lin, H. P.; Zhao, Q.; Liu, S. B.; Mou, C. Y. *Microporous Mesoporous Mater.* **2003**, *57*, 199. (c) Piwonski, I.; Zajac, J.; Jones, D. J.; Roziere, J.; Partyka, S.; Plaza, S. *Langmuir* **2000**, *16*, 9488. (d) Piwonski, I.; Zajac, J.; Jones, D. J.; Roziere, J.; Partyka, S. *J. Mater. Chem.* **1998**, *8*, 17. (e) Rachdi, F.; Hajji, L.; Goze, C.; Jones, D. J.; MairelesTorres, P.; Roziere, J. *Solid State Commun.* **1996**, *100*, 237.
(17) Anderson, M. W.; Shi, J. M.; Leigh, D. A.; Moody, A. E.; Wade, F. A.; Hamilton, B.; Carr, S. W. *J. Chem. Soc., Chem. Commun.* **1993**, 533.
(18) Hamilton, B.; Rimmer, J. S.; Anderson, M.; Leigh, D. *Adv. Mater.* **1993**, *5*, 583.
(19) Tseng, W. Y.; Lin, J. T.; Mou, C. Y.; Cheng, S. F.; Liu, S. B.; Chu, P. P.; Liu, H. W. *J. Am. Chem. Soc.* **1996**, *118*, 4411.
(20) Mehrotra, V.; Giannelis, E. P.; Ziolo, R. F.; Rogalskyj, P. *Chem. Mater.* **1992**, *4*, 20.
(21) Gournis, D.; Georgakilas, V.; Karakassides, M. A.; Bakas, T.; Kordatos, K.; Prato, M.; Fanti, M.; Zerbetto, F. *J. Am. Chem. Soc.* **2004**, *126*, 8561.

Table 1. Some Physical Properties and the Structural Formula of Laponite and the Two Montmorillonites (SWy and KUN)

clay	particle size (nm)	CEC[a] (molar equiv/100 g)	charge density (e^{-1}/unit cell)[b]	structural formula
Lap	20	48.1	0.5	$Na_{0.56}[Mg_{5.4}Li_{0.4}]Si_8O_{20}(OH)_4$
SWy	200	76.4	0.6	$Na_{0.62}[Al_{3.01}Fe(III)_{0.41}Mg_{0.54}Mn_{0.01}Ti_{0.02}](Si_{7.98}Al_{0.02})O_{20}(OH)_4$
KUN	200	119	0.9	$Na_{0.87}[Al_{3.12}Fe(III)_{0.20}Mg_{0.61}Ti_{0.01}](Si_{7.90}Al_{0.10})O_{20}(OH)_4$

[a] CEC is the cation exchange capacity. [b] Unit cell is the Si_8O_{20} unit.

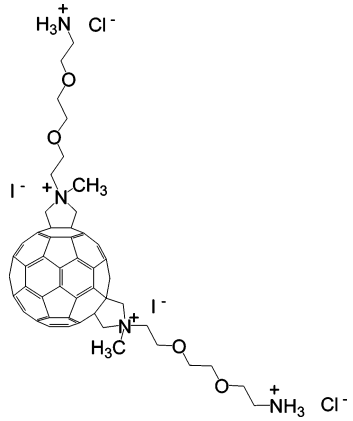

Figure 1. The water-soluble fulleropyrrolidine bisadduct derivative.

the Source Clay Minerals Repository, University of Missouri, Columbia. The clay was fractioned to $<2\ \mu$m by gravity sedimentation and purified by well-established procedures in clay science.[22] Sodium-exchanged samples (Na^+-SWy-1) were prepared by immersing the clay into 1 N solution of sodium chloride. Cation exchange was complete by washing and centrifuging four times with dilute aqueous NaCl. The samples were finally washed with distilled deionized water and transferred into dialysis tubes in order to obtain chloride-free clays and then dried at room temperature. The second clay, a synthetic sodium-saturated montmorillonite Kunipia F (KUN) was purchased from Kunimine Industries Co. (Japan). Finally, the third smectite was a synthetic trioctahedral hectorite, Laponite RD (Lap), produced by Laporte Industries Ltd. The chemical formulas and some properties of the three clays are summarized in Table 1.

Synthesis of the Water-Soluble Bisadduct Fullerene Derivative. The fullerene derivative (see Figure 1), referred here as bis-C_{60}, was prepared as previously reported.[14] Its solubility in water is 2×10^{-2} M.

Preparation of Clay/Bisadduct Fullerene Derivative Composites. A saturated brown-colored water solution of 2 mg of bis-C_{60} in water was mixed with a suspension of 5 mg of the corresponding layered materials in 2 mL of distilled water. This amount corresponds to 1, 1.4, and 2.2 times the CEC for KUN, SWy, and Lap clays, respectively. The mixtures were stirred at room temperature for 12 h (no color was observed at the supernatant after 2 h of stirring). The residue, separated by centrifugation, was washed five times by water and air-dried over a glass plate (products: bis-C_{60}/SWy, bis-C_{60}/KUN, and bis-C_{60}/Lap).

Powder X-ray Diffraction (XRD). The XRD patterns were collected on a D8 Advance Bruker diffractometer by using CuK_α (40 kV, 40 mA) radiation and a secondary beam graphite monochromator. The patterns were recorded in the 2-theta (2Θ) range from 2 to 80°, in steps of 0.02° and counting time of 2 s per step. Samples were in the form of films supported on glass substrates. For the preparation of the films, aqueous suspensions of bis-C_{60}/clay nanocomposites were deposited on glass plates, and the solvent was allowed to evaporate slowly at ambient temperature.

FTIR Spectroscopy. Infrared spectra were measured with a Bruker EQUINOX 55S infrared spectrometer, in the region of 400−4000 cm^{-1}, equipped with a deuterated triglycine sulfate (DTGS) detector. Each spectrum was the average of 200 scans collected at 2 cm^{-1} resolution. Samples were in the form of KBr pellets containing ca. 2 wt % sample.

X-ray Photoemission Spectroscopy (XPS). For the XPS measurements, evaporated gold films supported on glass (Arrandee, Germany) were used as substrates. They were cleaned in an ozone discharge (UV−Ozone Photoreactor TM PR100, Ultra Violet Products) for 15 min and sonicated in ethanol for 20 min immediately before being employed. Pure clays and clay/fullerene nanocomposites were dispersed in distilled deionized water (1 wt %), and after stirring and sonication for 30 min, a small drop of the suspension was left to dry in air onto the substrate. Additionally, bis-C_{60} alone (suspended in dichloromethane) was prepared in the same way as a reference material.

Samples were introduced via a load lock system into a SSX-100 (Surface Science Instruments) photoelectron spectrometer with a monochromatic AlK_α X-ray source ($h\nu = 1486.6$ eV). The base pressure in the spectrometer was 4×10^{-10} Torr during the measurement of bis-C_{60} and 1×10^{-9} Torr during the measurements of the clays and the bis-C_{60}/clay composites. The energy resolution was set to 1.16 eV to minimize measuring time. The photoelectron take off angle was 37°. An electron flood gun providing 0.3 eV kinetic energy electrons in combination with a Au grid placed 1 mm above the sample was used to compensate for sample charging. All binding energies of the clays and bis-C_{60}/clay composites were referenced to the Si 2s core level of smectite clay at 153.4 eV.[23] Binding energies of bis-C_{60} were referenced to the C 1s core level of the C_{60} cage at 285.2 eV.[24] For elements of bis-C_{60} inside the clay, the binding energies had to be corrected by +0.6 eV in order to compensate for the different final state screening caused by the negative charge of the clay surface. Spectral analysis included a Shirley background subtraction,[25] and peak deconvolution employing Gaussian−Lorentzian functions, in a least squares curve-fitting program (WinSpec) developed at the LISE, University of Namur, Belgium. For the N 1s line, however, we had to employ a linear background subtraction since low peak intensity did not allow for a Shirley background subtraction.

Transmission Electron Microscopy (TEM). A few milligrams of each bis-C_{60}/clay composite was dispersed in ethanol, and one droplet was put onto a holey carbon TEM grid, left to dry, and examined in a JEOL 200CX microscope working at 200 kV. The images are typical and representative of the samples under observation.

Laser Flash Photolysis. Nanosecond laser flash photolysis experiments were performed with laser pulses from a Qunta-Ray CDR Nd:YAG system (355 nm, 20 ns pulse width). All the experiments were performed at room temperature. Samples were prepared by depositing a drop of a 10 wt % aqueous suspension of bis-C_{60}/clay onto a 1 × 1 cm quartz substrate and processing it into a uniform film using a spin-coater (Chemat tech., KW-4A).

Computer Simulations. A model montmorillonite structure already used in a previous intercalation study [21] was set up. The unit cell was $Na[(Si_{16})(Al_7Mg)O_{40}(OH)_8]$ in the *P*1 space group (see cell coordinates in Supporting Information). The only atomic substitutions considered were Mg/Al (no Si/Al or Fe substitution). To identify the preferential anionic sites, several geometry optimizations were performed varying

(22) King, R. D.; Nocera, D. G.; Pinnavaia, T. J. *J. Electroanal. Chem.* **1987**, *236*, 43.
(23) Seyama, H.; Kinoshita, K.; Soma, M. *Surf. Interface Anal.* **2002**, *34*, 289.
(24) Maxwell, A. J.; Bruhwiler, P. A.; Nilsson, A.; Martensson, N.; Rudolf, P. *Phys. Rev. B* **1994**, *49*, 10717.
(25) Shirley, D. A. *Phys. Rev. B* **1972**, *5*, 4709.

the cations' distributions between the two separated surfaces and also varying the cations' initial distance from the surface. The best cation arrangement is characterized by half cations on one surface and the other half on the other delaminated surface. The cations lie in the hexagonal cavities. Periodic boundary conditions were applied, and the geometry was optimized with the only constraints of fixed OH distances and fixed *c* axis of the cell. The typical clay simulation cell—not the unit cell—contained 1458 plus one or more bis-C_{60}. The parameters were $a = 30.72$ Å, $b = 53.75$ Å, $c =$ dependent on the simulation, $\alpha = 90.0°$, $\beta = 99.1°$, $\gamma = 90.0°$. The *c* axis was varied in different simulations, but kept constant for a given simulation to modify the separation between the clay sheets. In practice, the simulation box contains a single clay platelet plus the molecules. The second clay layer was introduced through the periodic boundary conditions. Calculations were performed with a modified version of the Tinker[26] program, which has found several applications in our work.[12,27] The clays were described with a molecular mechanics force field that was used before for mica and clay interactions with organics.[21,28] Missing partial charges were calculated with the CHELPG model at the B3LYP/6-31G* level. They were $N_{pyridinium} = 0.237$, $C_{methyl} = -0.320$, $H_{methyl} = 0.155$ for a methylpyridinium and $N_{ammonium} = -0.244$, $H_{ammonium} = 0.313$, $C_{methyl} = 0.305$ for a methylammonium. Intercalation of the C_{60} bisadducts was achieved through the concomitant initial removal of the cations closest to the charged nitrogen atoms of the molecules. The subsequent calculations allowed the remaining cations to rearrange freely.

Results and Discussion

It is well-known that positively charged molecules can be introduced into the interlayer space of layered clay minerals by a simple ion exchange procedure. Charge balancing cations, such as Na^+, are replaced by the organic cations, and this is, in general, an easy and convenient method for the intercalation of organic cations soluble in water into the lamellar space of clay minerals. The newly introduced organic cations are held strongly by electrostatic forces between the large organic cations, and the negatively charged clay surfaces and the final conformation depend on the shape, size, and total charge of the organic cations and also on the charge density of the clay surface. The introduction of organic cations increases the organophilicity of the clay mineral and produces organoclays, which become dispersible in organic solvents.

In this work, three different clays of the smectite group with different structural and physical parameters were used, and the influence of these parameters on the fullerene adsorption was investigated. The three layered silicate clays show different layer charge density. Lap, a synthetic trioctahedral smectite, is characterized by relatively low CEC (0.48 molar equiv/g), while the CECs of the two montmorillonites, SWy-1 and KUN, are 0.76 and 1.19 molar equiv/g, respectively. Since exchangeable cations balance the negative surface charge, the CEC values reflect the density of the layer charge. Hence, Lap, SWy-1, and KUN represent the series of layered silicates of low, medium, and high charge densities, respectively. SWy-1 and KUN, though of different CECs, are similar structurally, having a dioctahedral configuration in octahedral sheets which is due to the presence of two occupied $AlO_4(OH)_2$ per one vacant octahedron. The negative layer charge of SWy-1 and KUN arises mainly from isomorphous substitutions of Al(III) by Mg(II) in octahedrons and only partially of Si(IV) by Al(III) in tetrahedrons.[2] Lap has trioctahedral configuration in octahedral sheets (three occupied octahedrons), and the negative layer charge arises from isomorphous substitutions of Mg(II) central atoms in $MgO_4(OH)_2$ polyhedrons by Li(I). The composition and structural differences affect acid/base properties of smectites. In dispersions, Laponite is more basic because of the hydrolysis of the octahedral sheets at the edges of the clay particle.[29] The basic properties of these clays were observed experimentally. We measured the pH of freshly prepared clay suspensions of the same concentrations (0.02 wt %). In the case of Lap, the pH was 9.8, a value significantly higher than those observed for KUN and SWy-1 suspensions of the same clay concentrations (9.0 and 7.8, respectively).

The incorporation of positively charged and highly soluble fulleropyrrolidine bisadduct into the interlayer space of the three unmodified clays (Na^+-homoionic forms) was carried out in aqueous clay suspensions. When Na^+-clay suspended in water was mixed with a brown-colored water solution of the ionic fulleropyrrolidine, the supernatant became colorless after 2 h of stirring at room temperature, indicating a successful and fast exchange. The protonated fullerene cations are readily adsorbed by ion exchange onto the clay surfaces. The monovalent Na^+-exchanged cations are replaced easily by the protonated fulleropyrrolidine molecules according to the reaction

$$\overline{\text{n Na}^+} + \text{bis-C}_{60}^{\,n+} \leftrightarrows \overline{\text{bis-C}_{60}^{\,n+}} + \text{n Na}^+$$

where the bold lines represent the clay platelets, which are estimated to have a thickness of 9.6 Å.[5] The preference of organic cations over alkali or alkaline earth cations on 2:1 layer silicate is attributed to the combined action of electrostatic forces between the large organic cations and the negatively charged clay surfaces and van der Waals interactions between the alkyl chains of the fullerene derivative and the siloxane surface.[30] X-ray diffraction measurements represent a powerful way to understand the changes in the interior of the clay microenvironment since the interlayer distance can be estimated by measuring the d_{001} spacing. The XRD data (Figure 2) show an increase of the basal spacings (d_{001}) of the three clays after insertion of bis-C_{60}. More specifically, in the case of SWy, the basal spacing d_{001}, which is 12.2 Å in the pristine clay, becomes 18.8 Å in the modified clay, which corresponds to an intersheet separation of $18.8 - 9.6 = 9.2$ Å. The diameter of C_{60} is ~7 Å. Each pyrrolidine ring, with its flexible side chain, must therefore occupy a space of slightly more than 1 Å. In practice, this makes it impossible for the rings to be perpendicular to either of the siloxane sheets that sandwich the molecule. Moreover, the distance between the methylated nitrogen of a pyrrolidine and the terminal amino group of the side chain is 8−9 Å, a value lower than the calculated 12.5 Å free distance

(26) (a) Dudek, M. J.; Ponder, J. W. *J. Comput. Chem.* **1995**, *16*, 791. (b) Ponder, J. W.; Richards, F. M. *J. Comput. Chem.* **1987**, *8*, 1016. (c) Kundrot, C. E.; Ponder, J. W.; Richards, F. M. *J. Comput. Chem.* **1991**, *12*, 402.
(27) (a) Baxter, R. J.; Teobaldi, G.; Zerbetto, F. *Langmuir* **2003**, *19*, 7335. (b) Biscarini, F.; Cavallini, M.; Leigh, D. A.; Leon, S.; Teat, S. J.; Wong, J. K. Y.; Zerbetto, F. *J. Am. Chem. Soc.* **2002**, *124*, 225. (c) Teobaldi, G.; Zerbetto, F. *J. Am. Chem. Soc.* **2003**, *125*, 7388.
(28) Cavallini, M.; Lazzaroni, R.; Zamboni, R.; Biscarini, F.; Timpel, D.; Zerbetto, F.; Clarkson, G. J.; Leigh, D. A. *J. Phys. Chem. B* **2001**, *105*, 10826.
(29) (a) Czimerova, A.; Bujdak, J.; Gaplovsky, A. *Colloids Surf., A* **2004**, *243*, 89. (b) Madejova, J.; Bujdak, J.; Janek, M.; Komadel, P. *Spectrochim. Acta, Part A* **1998**, *54*, 1397.
(30) (a) Johnson, C. T. In *CMS Workshop Lectures: Organic Pollutants in the Environment*; Sawhney, B. L., Ed.; The Clay Minerals Society: Boulder, CO, 1996; Vol. 8 p 1. (b) Gournis, D.; Deligiannakis, Y.; Karakassides, M. A.; Boussac, A.; Ioannidis, N.; Petridis, D. *Langmuir* **2002**, *18*, 10024.

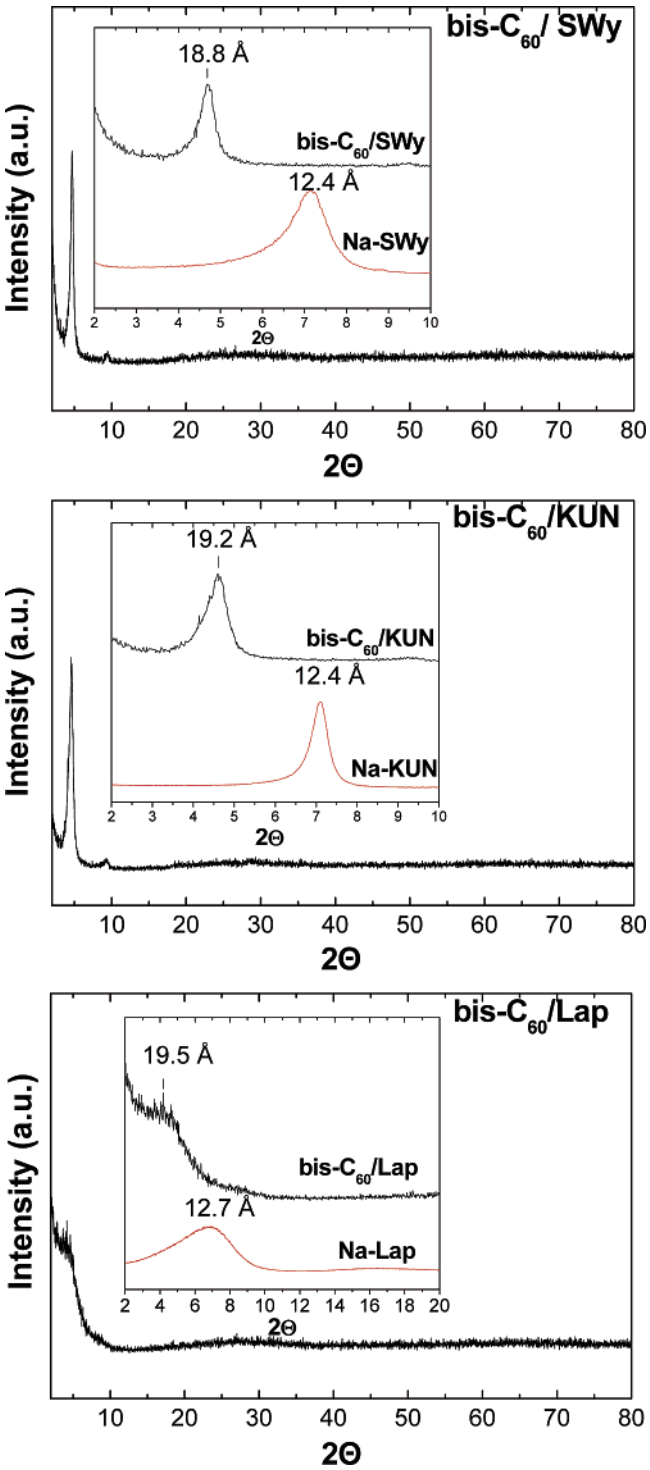

Figure 2. X-ray diffraction patterns of bis-C_{60}/nanocomposites.

between two negative sites in a clay with CEC of 80 molar equiv/100 g of clay.[31] The conclusion is that only one layer of protonated fullerene derivatives is accommodated between the montmorillonite layers and that the flexible organic chains must be lying almost parallel to the layers; see further discussion below. The results for the other clays are analogous. XRD pattern of bis-C_{60}/KUN shows a d_{001} spacing of 19.2 Å, which corresponds to an intersheet separation of 9.6 Å. The interlayer distance in this case is slightly higher than the SWy due to higher CEC of KUN montmorillonite. In the case of bis-C_{60}/Lap, the d_{001} peak is broad due to low aspect ratio of Laponite. Thus, the d spacing was calculated with relative low accuracy and found to be ~19.5 Å (interlayer space = 9.9 Å). Employing the Debye−Scherrer equation, $t = K\lambda/\beta \cos \theta$, where t is the crystalline thickness (or mean crystalline dimension), K is a constant near unity for clays ($K = 0.91$), λ is the wavelength of X-rays ($\lambda = 1.5418$ Å), θ is the angular position of the first diffraction peak, and β is the broadening of the 001 line diffraction line (calculated at full width at half of the peak height and expressed in radians), the crystalline thickness of the bis-C_{60}/clay nanocomposites can be estimated. The crystalline thickness was found 195.3, 151.8, and 44.9 Å for SWy, KUN, and Lap, respectively. The average stacking height of the layers can be estimated by the formula $N = t/d$, where N is the number of diffracting layers along the c axis and d is the 001 spacing of one layer (in Å). The average stacking height in the bis-C_{60}/SWy and bis-C_{60}/KUN systems was 11 and 8, respectively. In the case of bis-C_{60}/SWy, this value is almost doubled relative to pure SWy ($N = 5-6$). Interestingly, these values are remarkably larger, compared to other clay/organic systems. Clearly, the fullerene molecules play an important role in adjusting the layer spacing and hence improving the layer correlation length. However, the absence of higher order reflections (00l) suggests that the clay layers are not stacked in perfect registry, but that they have slipped sideways and are turbostratically disordered. Turbostratic is a type of crystalline structure where the basal planes have slipped sideways relative to each other, causing the spacing between planes to be greater than ideal. Similar turbostratic behavior has been observed in other layered materials, such as pyrolitic graphite and V_2O_5 xerogel.[32] The XPS analysis (see below) gave additional evidence for the existence of these turbostratic structures. Finally, in the case of bis-C_{60}/Lap system, the stacking height is poor ($N = 2$) due to low aspect ratio of Laponite.

Another important information derived from the XRD patterns of the three bis-C_{60}/clay nanocomposites was the absence of reflection peaks of the crystalline phase of bis-C_{60} in the 2Θ region 2−80°. This indicates that the bis-C_{60} molecules were not aggregated or absorbed on the external clay surfaces but lying in the interlayer space of the phyllomorphous materials.

The FTIR spectra of the bis-C_{60}/clay composites (Figure 3) present the characteristic bands of the fulleropyrrolidine bisadduct and of the clay, without significant changes, confirming the presence of bis-C_{60} in the clay minerals. Bis-C_{60}/SWy shows peaks at 3625 cm^{-1} (clay lattice −OH stretching vibrations), 3427 cm^{-1} (adsorbed H_2O deformation), 2918 and 2847 cm^{-1} ($-CH_2-$, $-CH_3$ stretching vibrations of fullerene organic chain), 1633 cm^{-1} (H_2O bending), 1460 and 1430 cm^{-1} ($-CH_2-$, $-CH_3$, and −NH bending vibrations), and 1052 cm^{-1} (clay lattice Si−O and Si−O−Si vibrations). Similar spectra are observed for the bis-C_{60}/KUN (bands at 3625, 3427, 2924, 2853, 1635, 1458, 1433, and 1048 cm^{-1}) and bis-C_{60}/Lap (bands at 3683, 3425, 2923, 2858, 1637, 1457, 1063, and 1009 cm^{-1}).

The starting materials (bis-C_{60}, SWy, KUN, Lap) and the produced bis-C_{60}/clay composites were studied using X-ray photoemission spectroscopy (XPS). XPS is a direct method to

(31) Szabo, A.; Gournis, D.; Karakassides, M. A.; Petridis, D. *Chem. Mater.* **1998**, *10*, 639.

(32) (a) Petkov, V.; Trikalitis, P. N.; Bozin, E. S.; Billinge, S. J. L.; Vogt, T.; Kanatzidis, M. G. *J. Am. Chem. Soc.* **2002**, *124*, 10157. (b) Petkov, V.; DiFrancesco, R. G.; Billinge, S. J. L.; Acharya, M.; Foley, H. C. *Philos. Mag. B* **1999**, *79*, 1519.

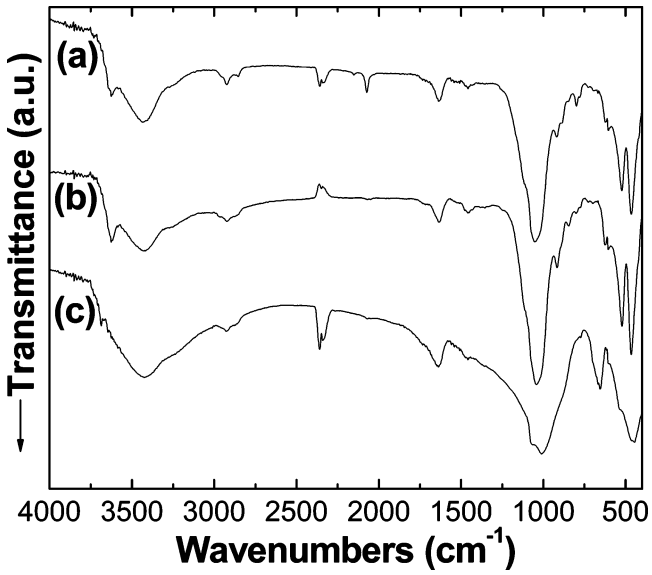

Figure 3. FTIR spectra of (a) bis-C_{60}/SWy, (b) bis-C_{60}/KUN, and (c) bis-C_{60}/Lap composites.

investigate how bis-C_{60} binds to the siloxane interface but also to give quantitative information about the elemental composition of the nanocomposites. This technique has been successfully applied to study the organic functionalization of C_{60},[33] as well as the interaction of organic molecules with clay minerals.[34] Figure 4 shows the XPS survey spectra of bis-C_{60} (a), bis-C_{60}/SWy (b), and Na−SWy (c). As labeled in spectrum (c), characteristic photoelectron and Auger peaks of O, Si, Al, and Mg are clearly distinguishable in pristine montmorillonite clay. A small carbon peak appears, mainly due to contamination from carbon species always present on the outer surface of air exposed materials,[35] but also due to soil organic matter present in the natural clay minerals.[36] After the insertion of bis-C_{60} (Figure 4b), a pronounced increase in the intensity of the carbon signal due to the presence of fulleropyrrolidine bisadduct inside the clay galleries is observed. On the other hand, the cross section for nitrogen is very low, and therefore it cannot be distinguished in the overview spectrum; however, detailed scans of the N 1s region (see below) clearly reveal its presence. The case is different for Cl and I anions: these elements are absent in the organoclay and cannot be detected even after detailed scans.

XP spectroscopy provides not only qualitative but also quantitative information; the peak areas normalized with the atomic sensitivity factors[37] are proportional to the amount of the corresponding atoms within the sampling depth. The chemical composition of pristine clays and bis-C_{60}/clay nanocomposites are given in Table 2. The relative atomic concentrations of the elements present in the pristine clays, calculated from XPS, are in agreement with the bulk atomic abundances of the elements obtained from the nominal compositions of Lap SWy and KUN (Table 1). The increase in the amount of carbon indicates the existence of the fullerene derivative in the final clay composites. The absence of chloride and iodide counterions in the bis-C_{60}/clay composites is an additional evidence of the intercalation of fulleropyrrolidine bisadduct inside the clay galleries since these anions cannot enter the negatively charged surfaces of the clay minerals. The positively charged nitrogen groups of bis-C_{60} are now balanced by the negative siloxane surfaces of the clay minerals. The most convincing evidence for the successful cation exchange process comes from the nitrogen signals in the bis-C_{60}/clay composites. From the amount of nitrogen, we can calculate how much bis-C_{60} is incorporated in the clay galleries. We find ~0.24, ~0.32, and ~ 0.17 bis-C_{60} molecules per formula unit of SWy, KUN, and Lap. If we consider four positive charges on the bis-C_{60} molecule, these amounts are 30−40% higher than expected from the CEC of the respective clays. There are two possible explanations of this behavior: (i) most probably, there is a partial deprotonation of the amine groups, which results in higher amount of adsorbed molecules, or (ii) this extra amount arises from bis-C_{60} hosted in the interlayer space of the clays in the form of physically adsorbed ion pairs.[31] To distinguish between these two possibilities, we focused on the N 1s photoemission signal.

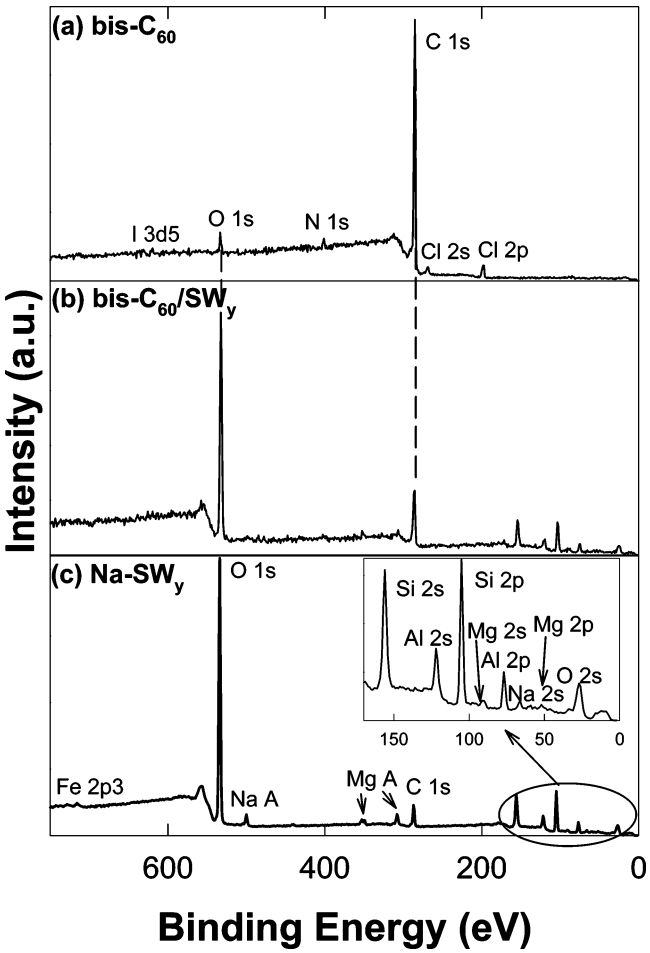

Figure 4. XPS survey spectra of (a) pure bis-C_{60}, (b) bis-C_{60}/SWy, and (c) pristine Na-SWy.

(33) (a) Sahoo, R. R.; Patnaik, A. *J. Colloid Interface Sci.* **2003**, *268*, 43. (b) Giovanelli, L.; Le Lay, G. *Appl. Surf. Sci.* **2000**, *162*, 513. (c) Huang, Y. Y.; Zhao, Y. L.; Gan, L. B.; Huang, C. H.; Wu, N. Z. *J. Colloid Interface Sci.* **1998**, *204*, 277.

(34) (a) Letaief, S.; Aranda, P.; Ruiz-Hitzky, E. *Appl. Clay Sci.* **2005**, *28*, 183. (b) Kuzniarska-Biernacka, I.; Silva, A. R.; Ferreira, R.; Carvalho, A. P.; Pires, J.; de Carvalho, M. B.; Freire, C.; de Castro, B. *New J. Chem.* **2004**, *28*, 853. (c) Du, J. X.; Wang, D. Y.; Wilkie, C. A.; Wang, J. Q. *Polym. Degrad. Stab.* **2003**, *79*, 319. (d) Ferreira, R.; Freire, C.; de Castro, B.; Carvalho, A. P.; Pires, J.; de Carvalho, M. B. *Eur. J. Inorg. Chem.* **2002**, 3032. (e) Fan, X. W.; Zhou, Q. Y.; Xia, C. J.; Cristofoli, W.; Mays, J.; Advincula, R. *Langmuir* **2002**, *18*, 4511.

(35) Barr, T. L. In *Practical Surface Analysis*, 2nd ed.; Briggs, D., Seah, M. P., Eds.; John Wiley: Chinchester, U.K., 1990; Chapter 8.

(36) Gournis, D.; Mantaka-Marketou, A. E.; Karakassides, M. A.; Petridis, D. *Phys. Chem. Miner.* **2001**, *28*, 285.

(37) Briggs, D.; Seah, M. P. *Practical Surface Analysis*; John Wiley: Chinchester, U.K., 1990.

Table 2. Chemical Atomic Compositions of Pristine Clays and Bis-C_{60}/Clays from XPS Experimental Data[a]

	Si 2p	Al 2p	Fe 2p	Mg 2p	O 1s	C 1s	N 1s
SWy	8.0	3.2 ± 0.1	0.30 ± 0.05	0.50 ± 0.05	23.7 ± 0.3	5.9 ± 0.1	
KUN	7.9	3.2 ± 0.2	0.10 ± 0.03	0.70 ± 0.05	25.7 ± 0.5	11.1 ± 0.5	
Lap	8.0			5.40 ± 0.1	23.6 ± 0.2	3.70 ± 0.07	
bis-C_{60}/SWy	8.0	3.10 ± 0.09	0.20 ± 0.02	0.60 ± 0.02	27.4 ± 0.1	17.1 ± 0.5	1.00 ± 0.05
bis-C_{60}/KUN	7.9	3.3 ± 0.1	0.10 ± 0.01	0.70 ± 0.04	26.1 ± 0.1	24.6 ± 0.7	1.30 ± 0.05
bis-C_{60}/Lap	8.0			5.3 ± 0.1	27.0 ± 0.2	14.9 ± 0.5	0.70 ± 0.03

[a] All the values normalized to Si assuming that Si corresponds to the nominal for each clay (Table 1).

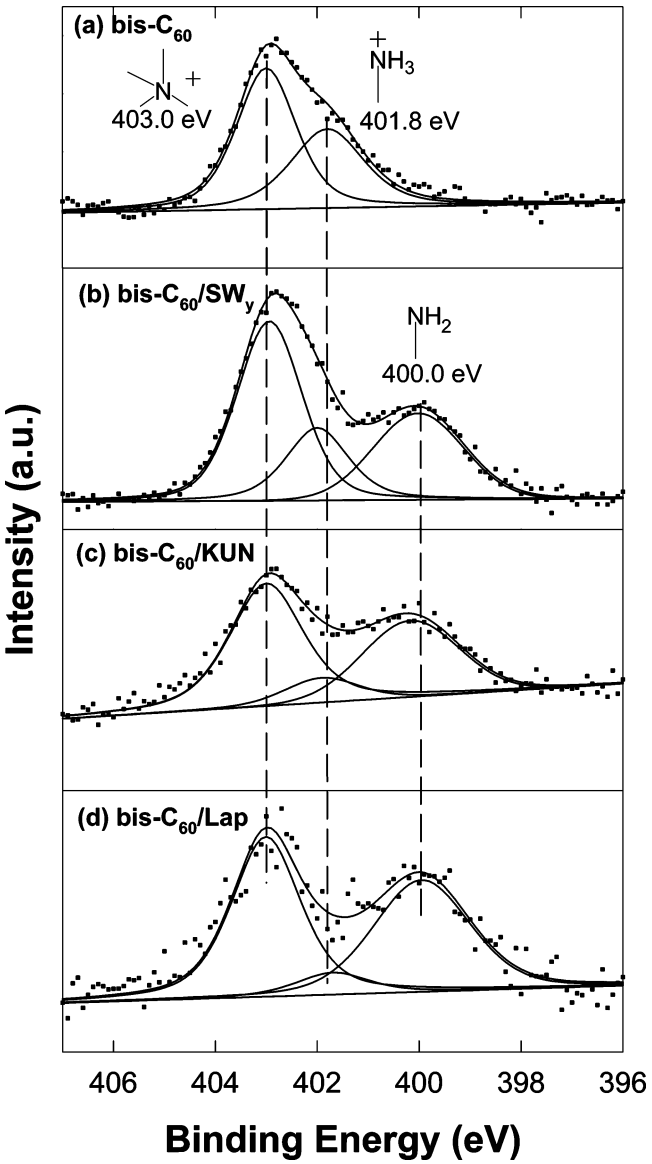

Figure 5. N 1s core level photoemission spectra of (a) pure bis-C_{60}, (b) bis-C_{60}/SWy, (c) bis-C_{60}/KUN, and (d) bis-C_{60}/Lap.

The knowledge of the chemical state of nitrogen in the clay/fullerene derivative composites is of great importance in order to understand the nature of the interactions between the clay surfaces and the positively charged nitrogen groups of the functionalized fullerene. Figure 5 shows the N 1s core level emission spectra of pure bis-C_{60} and of the three bis-C_{60}/clay composites. The spectrum of pure bis-C_{60} (Figure 5a) is fitted to the experimental data (constrained by the theoretical intensity ratio) assuming a molecule with two distinct chemically shifted N 1s core level emissions, occurring at 403.0 and 401.8 eV. The peak at 403.0 eV is assigned to the nitrogen of the pyrrolidinium group, while the peak at 401.8 eV is arising from the protonated amine end group ($-NH_3^+$) of bis-C_{60}.[38,39] On the other hand, the XPS spectra of bis-C_{60}/clay hybrids are composed of three nitrogen species occurring at 403.0, 401.8, and 400.0 eV. The existence of the new nitrogen species at 400.0 eV is attributed to neutral amine groups ($-NH_2$).[39,40] These groups are probably produced from deprotonation of the terminal alkylammoniums. The peaks arising from the pyrrolidinium nitrogen (403.0 eV) and of the terminal ammonium groups (401.8 eV) show, within the limit of error, the same binding energy values before and after the incorporation into the phyllomorphous matrix. Since chloride and iodide (counterions in untreated bis-C_{60}) are absent in the bis-C_{60}/clay nanocomposites and the binding energy values are indicating that the nitrogen groups present are still positively charged, it can be concluded that bis-C_{60} is strongly attached to the negatively charged siloxane surfaces of the clay minerals. According to our recent XPS studies on fullerene derivatives,[38] the type of the counterion of the pyrrolidinium nitrogen has no influence on the binding energy, which, in fact, gives additional support to the above finding. However, the peak at 400.0 eV resulting from the deprotonated ammonium group ($-NH_2$) in all three bis-C_{60}/clay composites is not present in the pure bis-C_{60}. As shown in Table 3, the relative area of the signal at 400.0 eV is increasing from 29% in bis-C_{60}/SWy to 36% in the bis-C_{60}/KUN and to a maximum of 44% in bis-C_{60}/Lap, corresponding to a reduction of the peak at 401.8 eV (21, 10, and 7%, respectively). This different behavior can be explained by the fact that the three smectites show different base activity in aqueous dispersions. Laponite in the aqueous suspension of our experiments is more basic (pH = 9.8) compared to KUN (pH = 9.0) and SWy (pH = 7.8) suspensions of the same clay concentrations (0.02 wt %). The high pH causes deprotonation of the terminal ammonium groups of the flexible chains, while the pyrrolidine nitrogens remain unaffected. Thus, in the case of Laponite, almost 90% of the ammonium groups are depro-

Table 3. Experimental Atomic Percentages Derived from the N 1s Photoemission Peak Areas of Bis-C_{60}/Clay Composites

	Binding energies		
	403.0 eV	401.8 eV	400.0 eV
bis-C_{60}/SWy	(50.0 ± 0.5)%	(21.0 ± 0.3)%	(29.0 ± 0.3)%
bis-C_{60}/KUN	(54.0 ± 0.3)%	(10.0 ± 0.1)%	(36.0 ± 0.2)%
bis-C_{60}/Lap	(49.0 ± 0.6)%	(7.0 ± 0.4)%	(44.0 ± 0.8)%

(38) Benne, D.; Maccallini, E.; Rudolf, P.; Sooambar, C.; Prato, M. *Carbon* **2005**, submitted.
(39) (a) Hooper, A. E.; Werho, D.; Hopson, T.; Palmer, O. *Surf. Interface Anal.* **2001**, *31*, 809. (b) Chernyshova, I. V.; Rao, K. H.; Vidyadhar, A.; Shchukarev, A. V. *Langmuir* **2000**, *16*, 8071. (c) Kowalczyk, D.; Slomkowski, S.; Chehimi, M. M.; Delamar, M. *Int. J. Adhes. Adhes.* **1996**, *16*, 227.
(40) Moulder, J. K.; Stickle, W. F. *Handbook of X-ray Photoelectron Spectroscopy*; Physical Electronics, Inc., 1995.

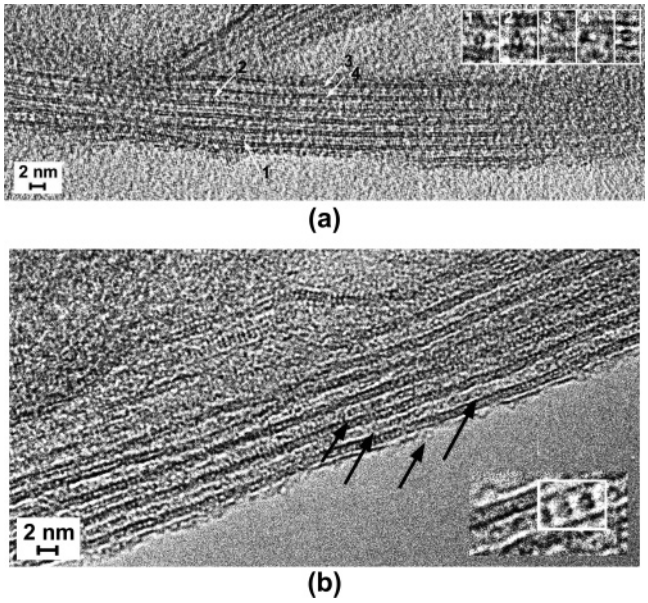

Figure 6. HRTEM images of (a) bis-C_{60}/KUN with the magnification of some intercalated C_{60} in inset and (b) bis-C_{60}/SWy nanocomposites with the comparison with C_{60} encapsulated in a carbon nanotube inside the white inset.

tonated. The deprotonation is also high in KUN (almost 70%). In the case of SWy, the more acidic environment keeps the deprotonation degree lower (60%) in comparison with the other two smectites. The information derived from these data is that the pyrrolidine group plays an important role for the insertion of bisadduct since the terminal ammonium can be partially deprotonated. This, actually, explains the high amount of loading of bis-C_{60} in the final composite materials since not all the nitrogen groups are positively charged. Additionally, we wish to emphasize that the $-NH_2$ derived XPS peaks are broader than the experimental resolution. This points to the existence of different components which cannot be resolved and which correspond to slightly different chemical environments for the nitrogen. Such a picture perfectly agrees with the hypothesis of a turbostratic order of the clay layers advanced before to explain the XRD data.

Undeniable proof for the successful intercalation of bis-C_{60} in the interlayer space of the clay minerals comes from the High-Resolution Transmission Electron Microscopy images. Figure 6 shows the HRTEM images of the bis-C_{60}/KUN (a) and the bis-C_{60}/SWy (b) nanocomposites. Both images show spherical objects imaged by dark circles with white dots in their centers that are consistent with C_{60} spheres intercalated between the clay platelets (for example, along the white arrows numbered from 1 to 4 in Figure 6a or along the black arrows in Figure 6b). It is not so evident to image the fullerenes due to the defocus and their small size; however, the size of the dark circles corresponds to the C_{60} diameter. To illustrate this fact, the comparison is made with fullerene C_{60} encapsulated in carbon nanotubes packed into bundles (inset image without number in Figure 6a and image inside the white inset in Figure 6b). The intersheet separation estimated from both images is in agreement with the XRD findings, while the high degree of stacking of the clay platelets, for both nanocomposites, is also confirmed. The bis-C_{60} molecules are not always centered with respect to neighboring clay platelets, as shown in inset images of Figure 6a; in image 1, the C_{60} sphere is in the center; in image 2, it is closer to one clay sheet, and in image 3, it is close to the other sheet.

Atomistic simulations can probe the interactions present in the composites. A number of initial structures were generated with coiled and uncoiled side chains of the bisadduct by rotation about the principal axis of inertia of the molecule. Unphysical structures, such as those requiring a very large interlayer distance, were discarded. For each of the 23 remaining structures (i) the 4 Na^+ closer to the ionic sites of the molecule were removed from the clay surface to reach cell neutrality, and (ii) a series of geometry optimizations starting from different *c* axis values (in steps of 0.5 Å at most) were performed. The results were considered stable when the same minimum was reached from interlayer distances larger and smaller than the final optimized one.

The minima have been found at an interlayer separation of ~11 Å, in fair agreement with the experimental value of ~9.2 Å. This is similar to what was found for pristine C_{60}.[21] The optimized structures cover a range of 104 kcal mol^{-1}. Figure 7 shows a cartoon with the main structural features of the more stable structures. Analysis of the structures shows that (1) the pyrrolidinium ions tend to interact with the same layer; (2) the ammonium ions tend to interact with the layer opposite to that of their pyrrolidinium; and (3) alkyl chains tend to interact with the clays.

The three propensity rules are in order of importance. With respect to the interactions with the surface, the low energy structures are characterized by large stabilizing interactions of the pyrrolidinium ions and the alkyl chain. The ammonium ions instead have sizable Coulombic interactions balanced by strong repulsion or low Coulombic interactions and weak repulsion. The high energy structures are obtained when the pyrrolidinium ions cannot establish binding Coulombic interactions.

The effect of additional intermolecular forces, when more than a single bis-C_{60} intercalates the layers, was explored with a larger cell of 1928 atoms and four embedded molecules. Figure 8 shows three illustrative cases obtained with extensive optimization and molecular dynamics simulations. To generate the structure, three criteria were followed. The first maximizes cage−cage and chain−chain interactions (Figure 8a). In the second, the alkyl chains are coiled around the cage and point in opposite directions (Figure 8b). The third is similar to the second, but the chain ends point to the same side of the cage (Figure 8c). Of the 18 structures that were generated with these criteria, the most stable is of the type given in Figure 8c and the second most stable is of the type given in Figure 8a. The two structures were also subjected to 100 ps of molecular dynamics, and the last snapshots are shown in Figure 9.

Although the three propensity rules obtained for the single intercalation are conserved, one should also add the preference of the side chains to interact with each other, a feature that appears clearly in Figure 9b, which is relative to the most stable structure.

To gain insight into electronic interactions (i.e., between individual bis-C_{60} or with the local clay environment), we tested the fullerene triplet excited state features and lifetimes in the bis-C_{60}/clay nanocomposites. In this context, we photoexcited the nanocomposite films—deposited onto a quartz substrate—with short 355 nm laser pulses. Differential absorption changes,

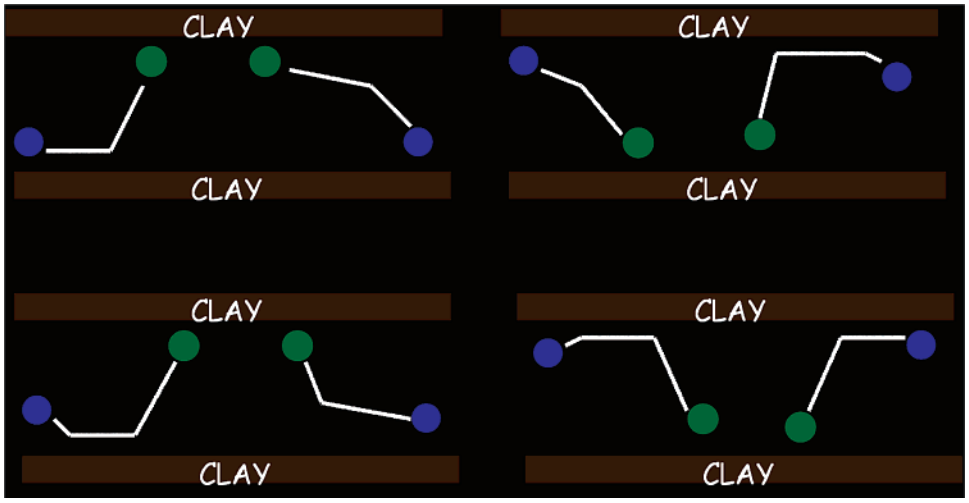

Figure 7. Cartoon of the locations of pyrrolidinium, ammonium, and alkyl chains in the more stable structures: green circles for pyrrolidinium; the blue circles for ammonium; white lines for alkyl chains; for clarity, C_{60} is not shown.

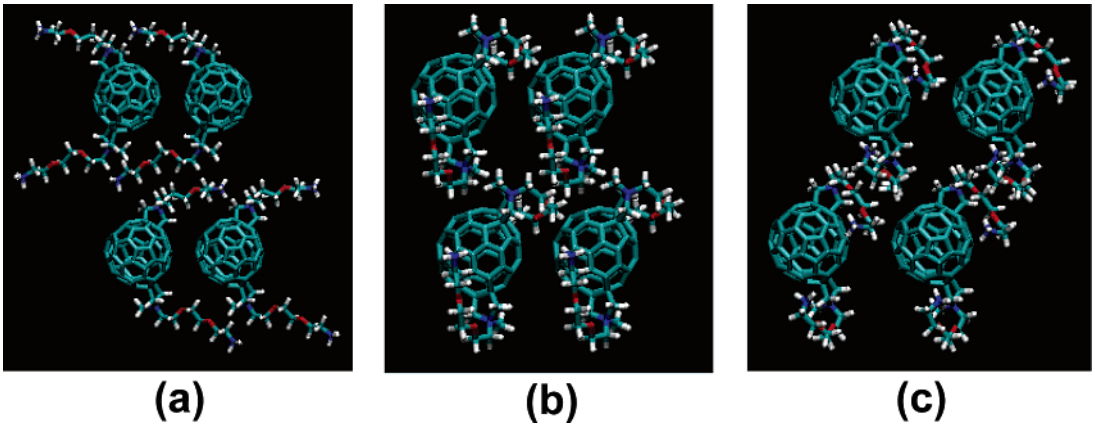

Figure 8. Top view of three structures of multiple bis-C_{60} intercalated between clay layers. The layers are not shown and are located below and on top of the molecules. For (a), (b), and (c), see text.

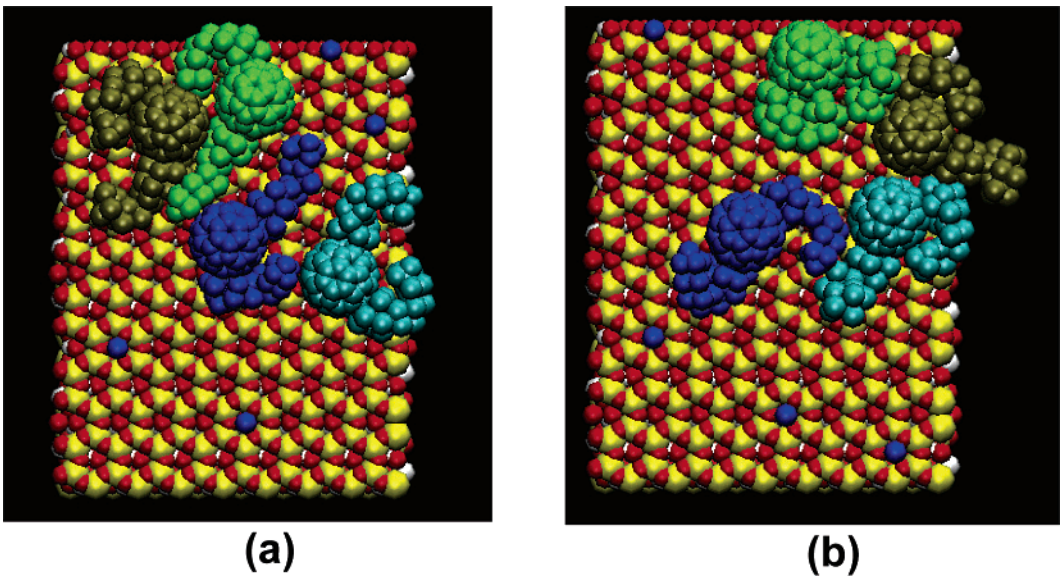

Figure 9. Low energy structures of intercalated bis-C_{60} after molecular dynamics: (a) this structure is obtained from initial conditions that maximize cage−cage and chain−chain interactions; (b) this structure was obtained from initial conditions with the alkyl chains coiled around the cage and the chain ends that point to the same side of the cage.

recorded with different time delays (i.e., 4.5×10^{-7}, 1.9×10^{-6}, 8.6×10^{-6}, and 2.1×10^{-5} s), are shown in Figure 10 and exhibit a strong maximum at 680 nm. In particular, they resemble the triplet−triplet features of bis-C_{60} in homogeneous aqueous solutions or in organic environments. Far more important is, however, the triplet lifetime since it reflects

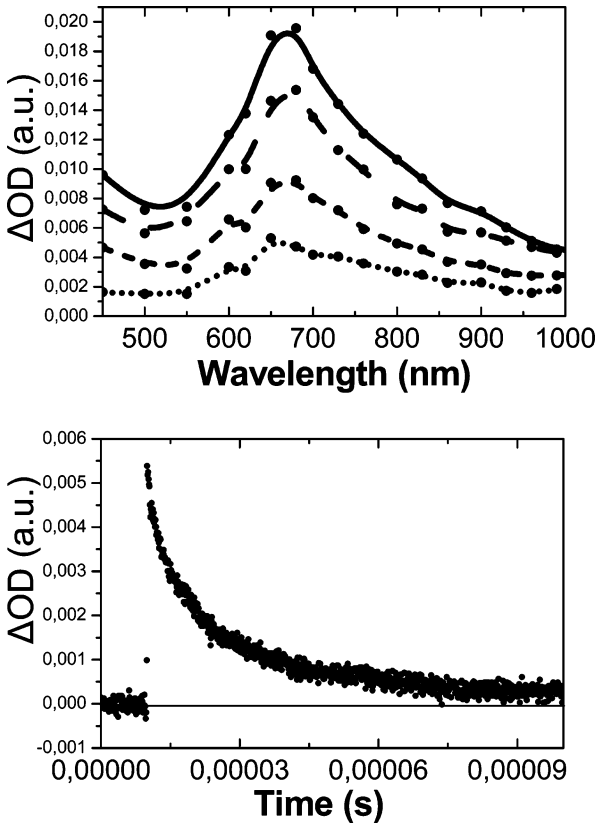

Figure 10. Top: differential absorption spectrum (visible and NIR) obtained upon nanosecond flash photolysis (355 nm) of bis-C_{60} intercalated into Laponite clay with time delays of 4.5×10^{-7} s (solid line), 1.9×10^{-6} s (dashed line), 8.6×10^{-6} s (short dashed line), and 2.1×10^{-5} s (dotted line) at room temperature. Bottom: time absorption profile at 700 nm.

electronic interactions (i.e., annihilation or energy/electron transfer quenching processes). We derived a monoexponential triplet lifetime of 23 μs (Figure 10) for the intercalated bis-C_{60} in Laponite. This value is (i) much longer than that typically seen in fullerene aggregates/clusters (i.e., submicroseconds),[41] (ii) in reasonable agreement with individual fullerene derivatives probed under similar conditions (i.e., concentration, laser intensity, temperature, etc.),[42] (iii) somewhat shorter than those found under conditions where bimolecular decay channels should be unimportant (i.e., ~50 μs).[43] In summary, our photophysical measurements help to corroborate the detailed microscopic investigation. In particular, the long-lived nature of the triplet excited states correlates well with the intercalation of individually and electronically separated bis-C_{60} molecules into smectite clays. Aggregates of bisfulleropyrrolidinium salts or electronically interacting fullerenes, on the other hand, would consequence triplet lifetimes on the order of only a few nanoseconds, due to rapidly occurring annihilation processes.

Conclusions

In conclusion, we have described the insertion and the subsequent behavior of a water-soluble bis-C_{60} into the interlayer space of three aluminosilicate-layered materials. Intercalation was performed in aqueous suspensions through a simple cation exchange reaction, and the final nanocomposites were characterized by several techniques. The bis-C_{60} molecules are lying in the interlayer space of the phyllomorphous materials, while the type of the host layered material strongly influences the chemical form, the amount, and the conformation of the guest fullerene molecules in the final composite materials. The reported materials constitute a new hybrid system and open new perspectives for the design and construction of novel C_{60}-based organic/clay hybrid materials.

Acknowledgment. This work was performed within the EU RT network CassiusClays Contract No. HPRN-CT-2002-00178 and received additional support from the Dutch Foundation for Fundamental Research on Matter (FOM), the Italian MIUR (PRIN 2004, prot. 2004035502), the Deutsche Forschungsgemeinschaft (SFB 583), FCI and the Office of Basic Energy Sciences of the U.S. Department of Energy. This research was supported in part also by the Breedtestrategie program of the University of Groningen. J.-F.C. is supported by the Belgian FNRS as Postdoctoral Researcher. The authors would like to acknowledge the use of the XRD unit of the Laboratory Network, UOI, and the EMAT laboratory (University of Antwerp) for the use of the microscope.

Supporting Information Available: Cartesian coordinates of the clay layer used in the simulations. This material is available free of charge via the Internet at http://pubs.acs.org.

JA0579661

(41) Guldi, D. M.; Hungerbuhler, H.; Asmus, K. D. *J. Phys. Chem.* **1995**, *99*, 13487.
(42) Guldi, D. M.; Prato, M. *Acc. Chem. Res.* **2000**, *33*, 695.
(43) Anthony, S. M.; Bachilo, S. M.; Weisman, R. B. *J. Phys. Chem. A* **2003**, *107*, 10674.